SHEAR BUCKLING ANALYSIS OF CORRUGATED WEB I-GIRDER WITH 3D NONLINEAR FINITE ELEMENT METHOD

Ni Putu Ary Yuliadewi[a], Heppy Kristijanto[a], Bambang Piscesa[a*], Priyo Suprobo[a], Faimun[a]

***Abstract**: This paper presents a shear buckling analysis of corrugated web I-girder beam using nonlinear finite element analysis. An in-house finite element package called 3D-NLFEA is used in the simulation. The steel material is modelled as solid elements with one-eight aspect ratio between the element size and its thickness. The double sine waves equation is used to generate the initial imperfection in the corrugated web. The nonlinear geometry deformation, which is essential in capturing the buckling behavior, is considered using the 2nd order analysis in 3D-NLFEA. A comparison with the carried out experimental test in the laboratory showed that the peak prediction from the analytical model was in good agreement. Furthermore, using the double sine waves equation as the initial imperfection can closely predict the buckling mode and shapes of the corrugated web I-girder as obtained from the experimental test.*

Keywords: *Corrugated web, double sine waves, imperfection, nonlinear finite element, shear buckling*

INTRODUCTION

The conventional steel I-girder is often used as a short-span railway bridge. Due to heavy load, high impact dynamic load factor, and fatigue, the depth of the steel I-girder is considerably higher than the standard I-girder available in the construction industry market. This I-girder is usually fabricated by combining steel plates using bolted or welded connection. One of the disadvantages of this steel I-girder is the buckling behavior of the web due to its slenderness. The buckling of the web can be prevented with closely spaced vertical stiffeners along the span of the I-girder are often used. As an alternative, corrugated web girders (with trapezoid or sinusoidal patterns) can be used to replace these closely spaced vertical stiffeners.

The use of a corrugated web I-girder can increase the out-of-plane rigidity without using vertical stiffener and thus increase the bending strength of the girder. In addition, the use of steel material can be reduced. From the aesthetic aspect of the structure, the use of the corrugated web is better than the conventional steel-plated girder [1]. The corrugated web plate thickness may vary from one to several millimeters. The corrugated web girders can have 9-13 percent less weight than the conventional steel-plated girder with stiffeners [2]. With the absence of vertical stiffener, the beam weight is reduced without compromising its strength and gains a reduced cost of about 30% [3].

Due to the accordion effect, when loaded in flexure, the corrugated web-only resists the shear forces. At the same time, the flanges carried out the compression and tension forces from the bending moment. The corrugated webs can have 1.5 to 2 times more shear buckling capacity than the conventional steel-plated girder. These shear forces can induce buckling in the web. The shear buckling in the corrugated web I-girder can be classified as local, global, and interactive shear buckling [2, 4-6]. It is well understood that the initial geometric imperfection can affect the shear strength and behavior of the corrugated web I-girder. The finite element simulation conducted by Elgaaly et al. [7] showed that numerical shear strength was higher than the test result.

[a]Civil Engineering Department, Institut Teknologi Sepuluh Nopember, Sukolilo, Surabaya 60111, Indonesia. Corresponding author email address: piscesa@ce.its.ac.id

Hassanein and Kharoob [1] evaluated the shear strength of corrugated web girder tested by [7] using ABAQUS. In their study, the initial imperfection was modeled using the scaled deformed shape of the first buckling mode. The peak was able to be accurately predicted. However, the mid-span deflection at peak load was predicted much less than the test result. In addition, the behavior of the post-peak response from ABAQUS showed a snap-back behavior which was not found in the recorded load-deflection shape in the test result.

In this paper, a numerical simulation to predict the shear buckling behavior of the corrugated web I-girder is carried out using an in-house 3D-NLFEA finite element package. 3D-NLFEA was developed by Piscesa et al. [8-10]. The 3D-NLFEA can model the random materials, initial geometric imperfections, and 2nd order analysis. The 3D-NLFEA package uses SALOME 9.3.0 [11] as the pre-processor and ParaView 5.8.0 [12] as the post-processor. For validation purposes, one corrugated web I-Girder tested at the Laboratory of Structure (Civil Engineering Department, Institut Teknologi Sepuluh Nopember, Surabaya, Indonesia) is used in this study.

RESEARCH SIGNIFICANCE

This paper presents a shear buckling analysis of corrugated web I-girder using an in-house 3D-NLFEA finite element package. The model is verified with one of the tested specimens in the laboratory. The initial geometric imperfection is generated using the double sine wave equation. This paper also investigates the sensitivity of the initial geometric imperfection to the load-deflection curve and the buckling deformation shape.

METHODOLOGY

The research methodology starts with modeling the corrugated web I-girder and investigates the behavior without using any initial geometric imperfection. The predicted load-deflection curve is then compared with the test result. The expected peak load generally higher than the test result. To scaled-down the expected peak load, initial geometric imperfection must be initiated before the analysis. The initial geometric imperfection considered in the study is generated using a double sine waves equation. With the initial geometric imperfection, the predicted load-

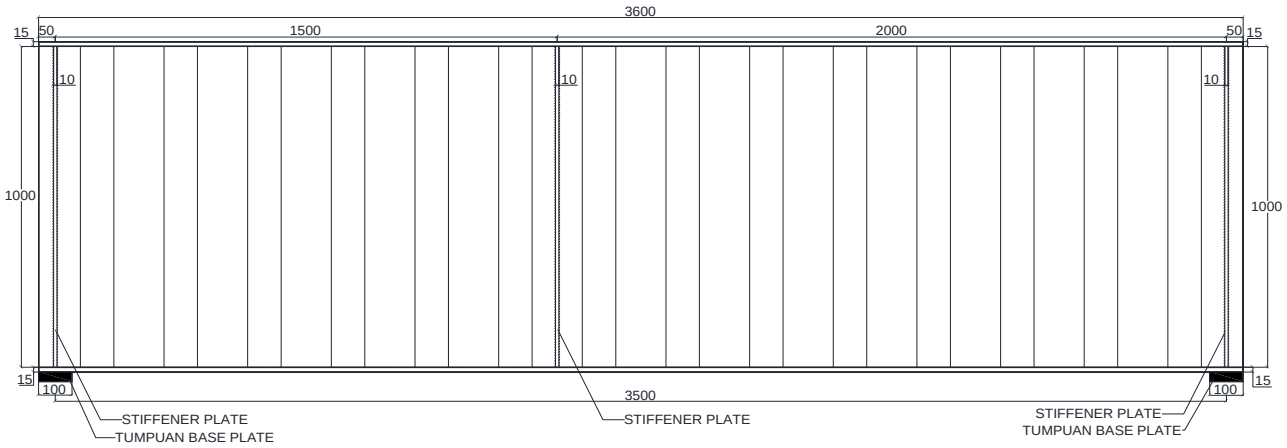

Figure 1 The geometry details of the modeled SCWG-I specimen (mm)

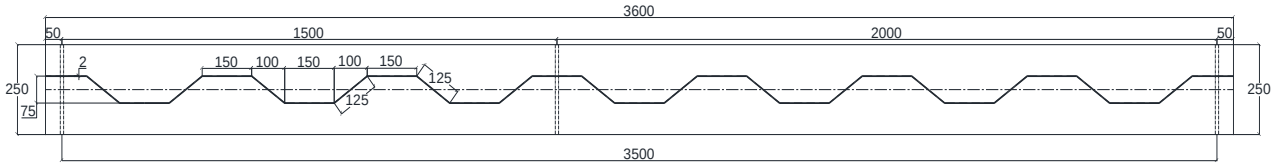

Figure 2 The corrugation dimension of the modeled SCWG-I specimen (mm)

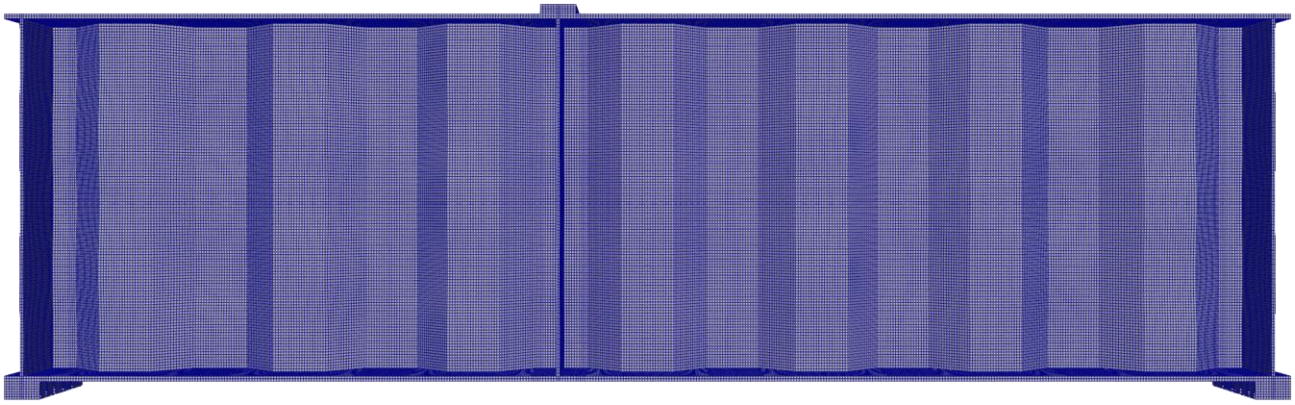

Figure 3 The meshing of the modeled SCWG-I specimen (side view)

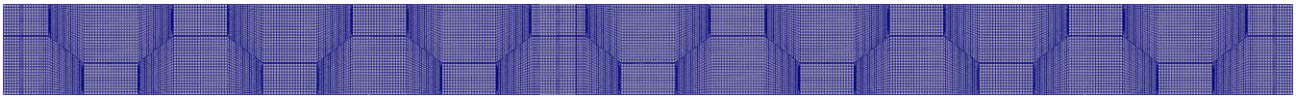

Figure 4 The meshing of the modeled SCWG-I specimen (top view)

deflection curve and the buckling shape of the specimen are compared with the test result. For sensitivity analysis, some length parameters in the double sines wave equation are also investigated to find the best result that matches the buckling shape of the tested specimen. Details on the research methodology are discussed in the following section.

A. SPECIMEN GEOMETRY, 3D MODELING, AND MATERIAL PROPERTIES

Figure 1 shows the side view of the modeled specimen. The total beam, span, and height lengths are 3600, 3500, and 1000 mm, respectively. The corrugated web thickness is 2 mm. Ten-millimeter thick stiffeners are provided at the supports and at the load location to prevent buckling at those locations. Figure 2 shows the top mid-height view of the specimens. The corrugation width (b), depth (h_r), and incline length (d) are 150, 75, and 100 mm, respectively.

The three-dimensional model is prepared using SALOME 9.3.0 [13] software which serves as the pre-processor. All the boundary conditions (at nodes) and grouping of material for a further assignment are done in SALOME 9.3.0. The specimen is modeled using the hexahedral element with BBar element technology [14]. Figures 3 and 4 show the specimen meshed model (side and top views). The maximum mesh size of the model is set to eight mm, which gives the ratio of element length to element thickness (L_e/t) less than equal to four. By using the predefined maximum mesh size, the total number of hexahedral elements is 181,590 elements and the total nodal element is 303,968 nodes.

Simply supported boundary condition is used where the support on the left-hand side is assigned as a hinge, and the right-hand side's support is set as a roller. The load is controlled using displacement at the loading point. The input from SALOME 9.3.0 is then extracted to Microsoft

Excel files to further process the initial geometric imperfection and assign material properties to the elements. The steel material grade is equivalent to ST37 with a yield strength of 240 MPa and the ultimate yield strength of 370 MPa. The Young's modulus of the steel material is set to 210 GPa. Once the input is ready, the input file is executed using the 3D-NLFEA finite element package. Once the simulation is completed, the output is viewed using ParaView 5.9.0 [12, 15, 16].

B. INITIAL GEOMETRIC IMPERFECTION

The initial geometric imperfection is compulsory to capture the buckling mode of the modeled specimen. An error can cause this initial geometry during the fabrication process of the I-Girder. In addition, the welding process can also leave some residual stresses, which also causes some material imperfection. During the welding process, some restrained deformation due to the yielding of the plates also takes place. Although considering these imperfection possibilities in the analysis would be beneficial, the imperfection is limited only to the initial geometric defect in this study.

The initial geometric imperfection is considered as the out-of-plane deformation of the corrugated web. This out-of-plane deformation, as proposed by Elgaaly et al. [17] has the form of double sine waves and is:

$$z_{(x,y)} = z_0 \times \sin\left(\frac{\pi x}{a}\right) \times \sin\left(\frac{\pi y}{h}\right) \quad (1)$$

In Eq. (1), a is the horizontal length of one sine wave, h is the vertical length of one sine wave, x is the distance measured from the outer left position of the beam, y is the distance measured from the lowest elevation of the corrugated web, and z_0 is the amplitude of the sine.

RESULTS AND DISCUSSION

Figure 5 shows the comparison of the load-deflection curve between the model (without initial geometric imperfection) and the test result. From Figure 5, it is seen that the peak load of the tested specimen is 468.52 kN and the displacement at the peak load is 4.578 mm. On the other hand, the predicted peak load using 3D-NLFEA without considering the initial geometric imperfection gives the peak load 500.16 kN, and the displacement at the peak load is 6.3 mm. The ratio between the predicted peak load to the test result is 1.068.

For the analysis that considers the initial geometric imperfection using the double sine waves, four variations in the horizontal and vertical lengths of the sine waves are investigated. Table 1 shows the variation in the horizontal length of the sine wave (a) while the vertical height of the sine wave remains constant. Table 1 also showed the scaled deformation, maximum sine amplitude, and the predicted peak load for each variation in a. Table 2 shows the different values on the vertical length of the sine wave (h) while the horizontal length of the sine wave remains constant. The scaled deformation, maximum sine amplitude, and the predicted peak load are also shown in Table 2. The scaled deformation magnitudes are selected such that the predicted peak load is almost equal to the peak load from the test result.

Figure 6 shows the comparisons of the load-displacement curve between the model with the parameter defined in Table 1 and the test result. As shown in Figure 6, the load-deformation behavior after the post-peak is almost similar. However, the obtained buckled shapes for each of the variation differs significantly. Figure 7, Figure 8, Figure 9, and Figure 10 show the deformed buckling shape for each variation listed in Table 1.

Table 1 Effect of variation in a and its respective scaled deformation magnitude to the predicted peak load

		Imperfection		
a (mm)	h (mm)	Scaled deformation magnitude	Maximum amplitude (mm)	Peak Load (kN)
200	200	95.00%	1.90	468.95
250	200	142.0%	2.84	468.12
300	200	150.0%	3.00	468.50
350	200	183.2%	3.66	468.50

Table 2 Effect of variation in h and its respective scaled deformation magnitude to the predicted peak load

		Imperfection		
a (mm)	h (mm)	Scaled deformation magnitude	Maximum amplitude (mm)	Peak Load (kN)
350	200	183.2%	3.66	468.95
350	250	171.0%	3.42	468.53
350	300	188.0%	3.76	468.63
350	350	193.0%	3.86	468.42

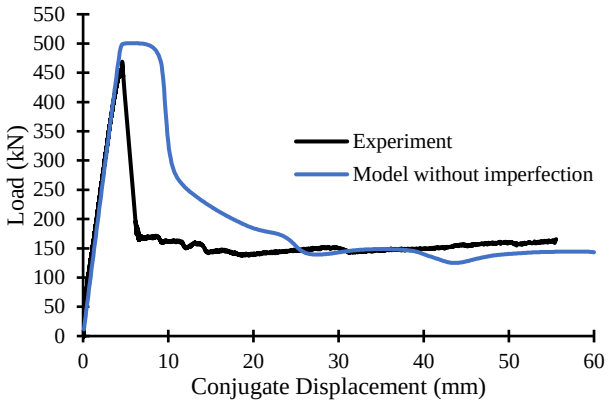

Figure 5 Comparison of the predicted load-displacement curve with the test result

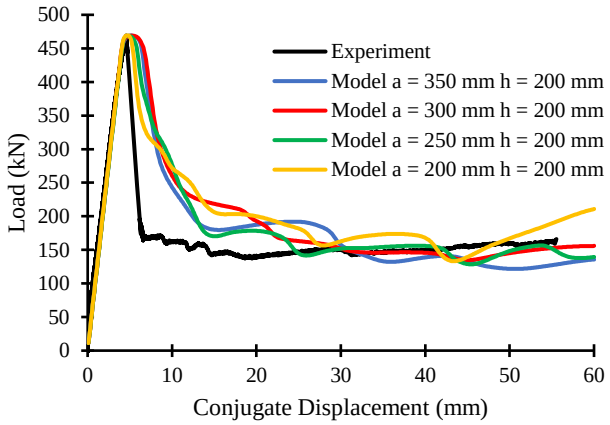

Figure 6 Effect of variation in a to the load-displacement curve

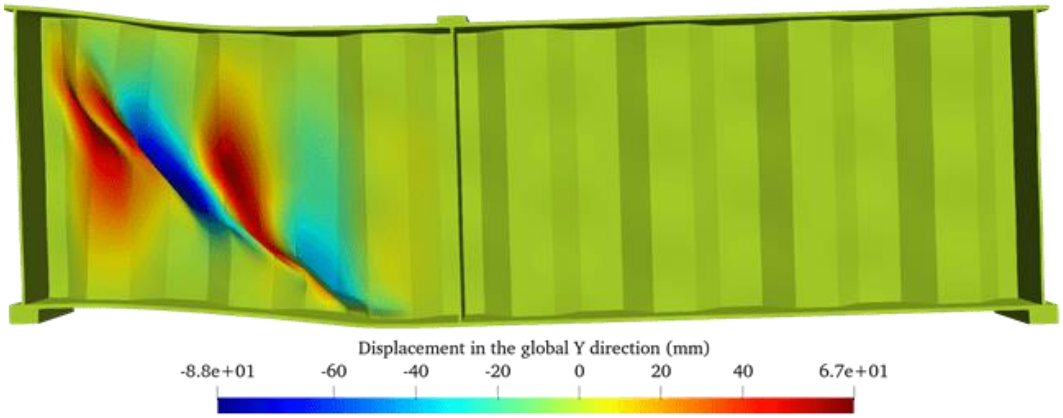

Figure 7 The buckling deformed shape of the specimen with a = 350 mm and h = 200 mm

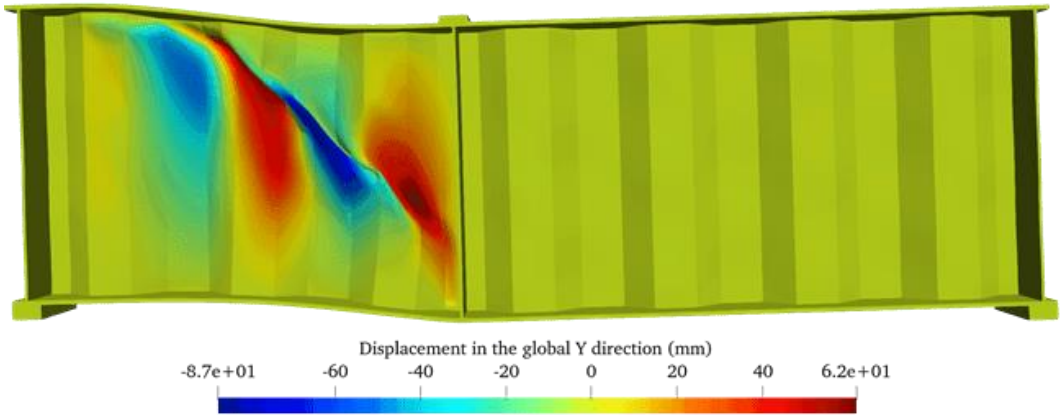

Figure 8 The buckling deformed shape of the specimen with a = 300 mm and h = 200 mm

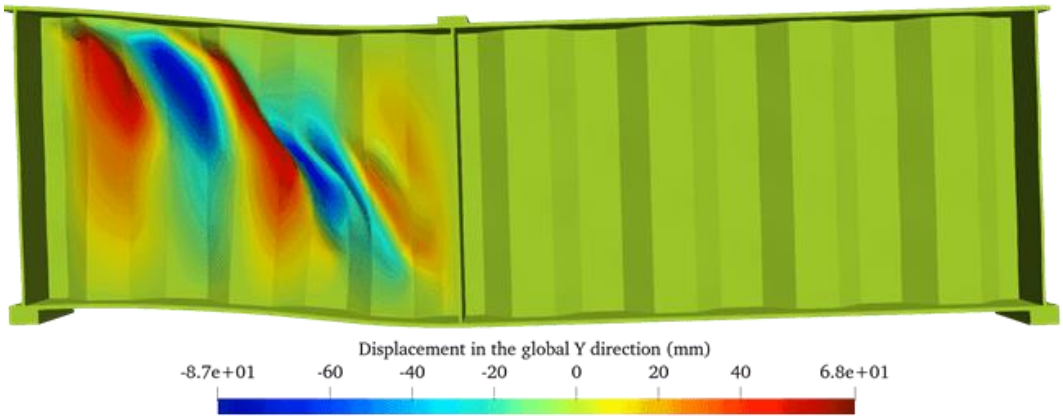

Figure 9 The buckling deformed shape of the specimen with a = 250 mm and h = 200 mm

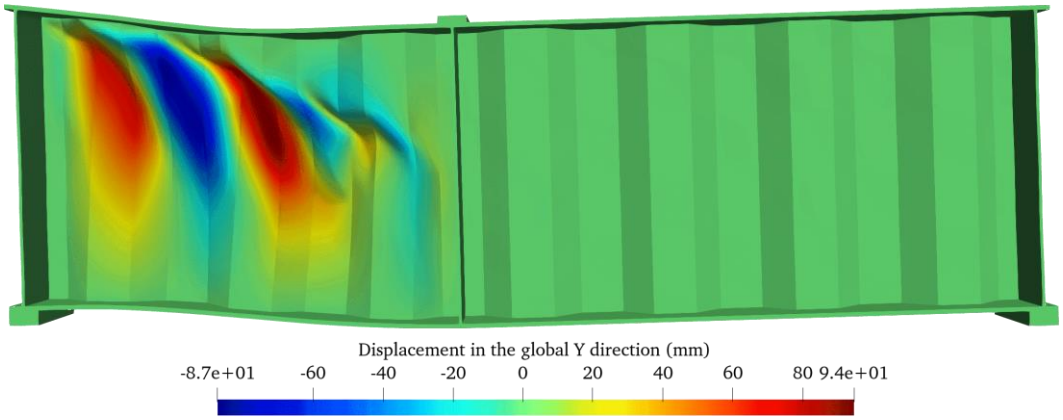

Figure 10 The buckling deformed shape of the specimen with a = 200 mm and h = 200 mm

Figure 11 The buckling deformed shape of the tested specimen

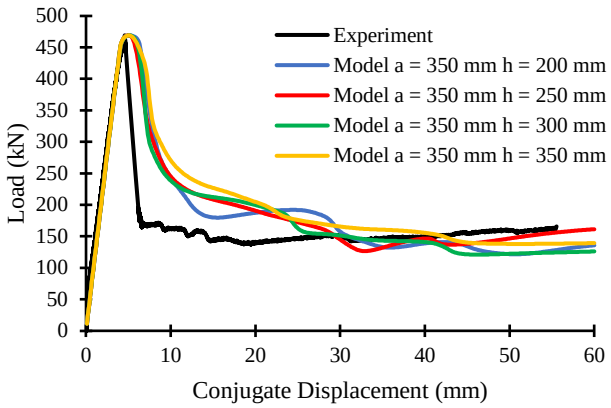

Figure 12 Effect of variation in *h* to the load-displacement curve

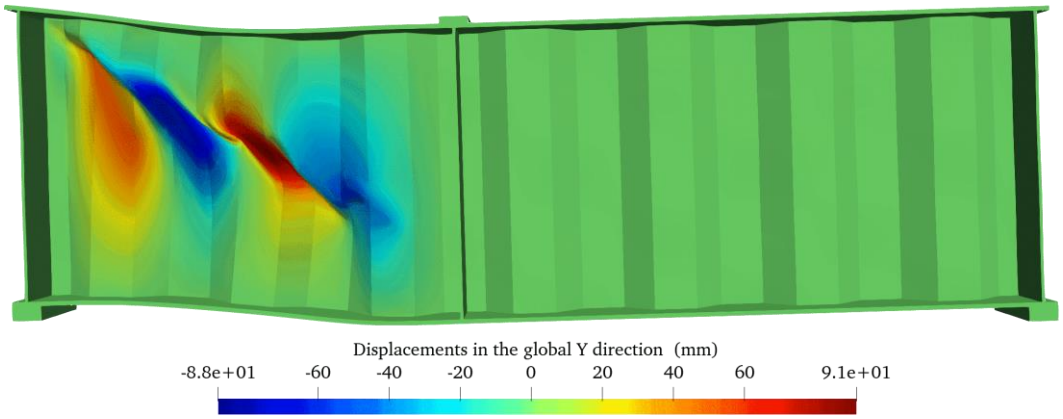

Figure 13 The buckling deformed shape of the specimen with *a* = 350 mm and *h* = 250 mm

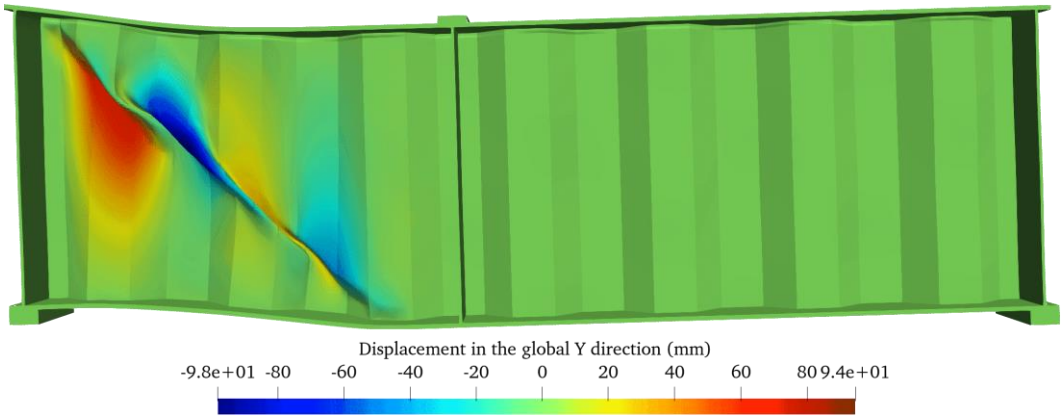

Figure 14 The buckling deformed shape of the specimen with *a* = 350 mm and *h* = 300 mm

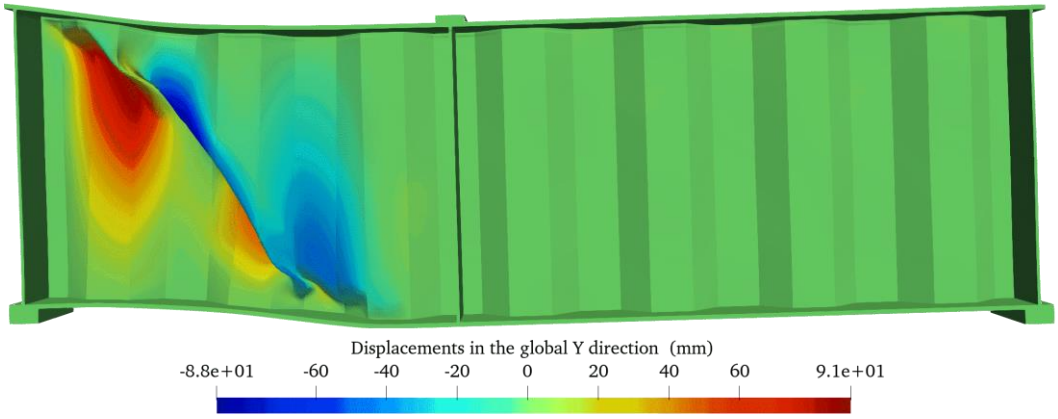

Figure 15 The buckling deformed shape of the specimen with *a* = 350 mm and *h* = 350 mm

To choose the most suitable value for *a*, it is suggested to look at the deformed buckling shape of the tested specimen. Figure 11 shows the deformed buckling shape of the tested sample. As shown in Figure 11, the deformed buckling shape is categorized as the interactive buckling mode. In the interactive buckling mode, web buckled involving multiple folds [21]. In the tested specimen, the buckling shape of the web started from the top left corner below the top flange and propagated in a diagonal direction towards the bottom flange. By comparing the predicted buckling deformed shape with the test result, the closest predicted buckling deformed shape is associated with the value of *a* equal to 350 mm (see Figure 7).

Figure 12 shows the predicted load-displacement behavior with the parameter defined in Table 2. A similar conclusion with Figure 11 was obtained. The obtained buckling deformed shape is shown in Figure 13, Figure 14, and Figure 15, with the value of *h* equal to 250, 300, and 350 mm, respectively. For a value of *h* equal to 200 mm is already shown in Figure 7. As shown in Figure 7, Figure 13, Figure 14, and Figure 15, the closest predicted buckling deformed shape with the test result was associated with Figure 7. Therefore, it can be concluded that the values for a and h that give the closest prediction of the deformed buckling shape with the test result are 350 and 200 mm, respectively.

CONCLUSIONS

This paper presented a numerical simulation to capture the shear buckling behavior of the corrugated web I-Girder using a 3D-NLFEA finite element package. The analysis without and with initial geometric imperfection was carried out. For the analysis with initial geometric imperfection, double sine waves equation was used to generate the initial geometric imperfection. Variation for both the horizontal and vertical lengths of the sine wave equation was observed to find out the best values that able to predict well the deformed buckling shape of the modeled specimen.

The predicted peak load was higher than the peak load from the test result from the analysis without initial geometric imperfection. While from the study with initial geometric imperfection can match the peak load from the test result with different scaled deformation values for each of the considered variations in the initial geometric imperfection. The parametric study found out that the value that matched well the deformed buckling shape of the test result for the vertical and horizontal length of the double sine waves equation are 350 and 200 mm, respectively. Using the appropriate double sine wavelengths, the scaled deformation magnitude that gives predicted peak load equal to the peak load from the test is 183.2%. The associated maximum amplitude for the selected, scaled deformation magnitude is 3.664 mm.

REFERENCES

[1] M. F. Hassanein and O. F. Kharoob, "Behavior of bridge girders with corrugated webs: (II) Shear strength and design," *Engineering Structures*, vol. 57, pp. 544-553, 2013.

[2] M. Leblouba, M. T. Junaid, S. Barakat, S. Altoubat, and M. Maalej, "Shear buckling and stress distribution in trapezoidal web corrugated steel beams," *Thin-Walled Structures*, vol. 113, no. December 2016, pp. 13-26, 2017.

[3] K. Aggarwal, S. Wu, and J. Papangelis, "Finite element analysis of local shear buckling in corrugated web beams," *Engineering Structures*, vol. 162, no. May, pp. 37-50, 2018.

[4] J. Moon, J. W. Yi, B. H. Choi, and H. E. Lee, "Lateral-torsional buckling of I-girder with corrugated webs under uniform bending," *Thin-Walled Structures*, vol. 47, no. 1, pp. 21-30, 2009.

[5] M. F. Hassanein and O. F. Kharoob, "Behavior of bridge girders with corrugated webs: (I) Real boundary condition at the juncture of the web and flanges," *Engineering Structures*, vol. 57, pp. 554-564, 2013.

[6] F. Riahi, A. Behravesh, M. Y. Fard, and A. Armaghani, "Shear buckling analysis of steel flat and corrugated web I-girders," *KSCE Journal of Civil Engineering*, vol. 22, no. 12, pp. 5058-5073, 2018.

[7] R. G. Driver, H. H. Abbas, and R. Sause, "Shear behavior of corrugated web bridge girders," *Journal of Structural Engineering*, vol. 132, no. 2, pp. 195-203, 2006.

[8] B. Piscesa, M. M. Attard, D. Prasetya, and A. K. Samani, "Modeling cover spalling behavior in high strength reinforced concrete columns using a plasticity-fracture model," *Engineering Structures*, vol. 196, no. October 2018, p. 109336, 2019.

[9] B. Piscesa, M. M. Attard, and A. K. Samani, "Three-dimensional finite element analysis of circular reinforced concrete column confined with FRP using plasticity model," *Sustainable Civil Engineering Structures and Construction Materials*, vol. 194, p. 109336, 2018.

[10] B. Piscesa, M. M. Attard, D. Prasetya, and A. K. Samani, "Modeling cover spalling behavior in high strength reinforced concrete columns using a plasticity-fracture model," *Engineering Structures*, vol. 196, p. 109336, 2019.

[11] "SALOME: The Open Source Integration Platform for Numerical Simulation." http://www.salome-platform.org/

[12] J. Ahrens, B. Geveci, and C. Law, "ParaView : An end-user tool for large-data visualization," in *The visualization handbook*, vol. 717, 2005.

[13] *SALOME - The Open Source Integration Platform for Numerical Simulation. http://www.salome-platform.org/*. (2019). [Online]. Available: http://www.salome-platform.org/

[14] T. J. Hughes, *The finite element method: linear static and dynamic finite element analysis*. Courier Corporation, 2012.

[15] J. Ahrens, B. Geveci, C. Law, C. Hansen, and C. Johnson, "36-ParaView: An end-user tool for large-data visualization," *The Visualization Handbook*, p. 717, 2005.

[16] U. Ayachit, "The paraview guide: a parallel visualization application," 2015.

[17] M. Elgaaly, R. W. Hamilton, and A. Seshadri, "Shear strength of beams with corrugated webs," *Journal of Structural Engineering*, vol. 122, no. 4, pp. 390-398, 1996.

[18] X. Cao, Y. Xu, M. Wang, G. Zhao, L. Gu, and Z. Kong, "Experimental study on the residual stresses of

800 MPa high strength steel welded box sections," *Journal of Constructional Steel Research,* vol. 148, pp. 720-727, 2018.
[19] M. Khan, A. Paradowska, B. Uy, F. Mashiri, and Z. Tao, "Residual stresses in high strength steel welded box sections," *Journal of Constructional Steel Research,* vol. 116, pp. 55-64, 2016.
[20] T. Le, A. Paradowska, M. A. Bradford, X. Liu, and H. R. Valipour, "Residual stresses in welded high-strength steel I-Beams," *Journal of Constructional Steel Research,* vol. 167, p. 105849, 2019.
[21] J. Yi, H. Gil, K. Youm, and H. Lee, "Interactive shear buckling behavior of trapezoidally corrugated steel webs," *Engineering Structures,* vol. 30, no. 6, pp. 1659-1666, 2008.